Ultrafast Exciton-to-Polaron Conversion in Densely Packed Small Organic Semiconducting Molecules

*Oleg V. Kozlov, Yuriy N. Luponosov, Alexander N. Solodukhin, Bruno Flament, Yoann Olivier, Roberto Lazzaroni, Jérôme Cornil, Sergei A. Ponomarenko, and Maxim S. Pshenichnikov**

In the rapidly developing field of organic photovoltaics, the material design and device engineering are key factors that eventually determine the device efficiency. Design of the active layer material and intermolecular interactions largely determine the efficiency of organic solar cells. In this study, the authors discuss ultrafast photophysics of four star-shaped molecules (SSMs) as benchmark materials with time-resolved photoinduced absorption and photoluminescence spectroscopy as experimental tools. The authors show that efficient exciton-to-charge conversion occurs in SSM films even without an external acceptor. This results in the lowering of the Coulomb binding between intermolecular electron–hole polaron pairs which, in turn, can lead to an increased open-circuit voltage. The findings suggest that promoting intermolecular interactions in films of small organic molecules is one of the pathways to highly efficient organic solar cells.

1. Introduction

The efficiency of organic optoelectronic devices essentially depends on two main factors: the photophysical and chemical properties of the materials[1–9] and the optimization of the device structure.[7,10–13] Even though both factors are of high importance, the properties of the materials might be considered as prevailing: it is impossible to make an efficient device out of poorly designed materials. Therefore, the optimization of the material design and understanding the structure–property relationship are burning issues in materials sciences.[14–16]

Nowadays, among the most popular donor materials for organic solar cells (OSCs) are push–pull small molecules (SMs).[7,10,17–23] Optimized devices based on SMs have already broken the 10% threshold in power conversion efficiency with a great potential for further improvement.[7,19,24,25] The best results of >10% efficiency for solution-processed OSCs were achieved using relatively complex and difficult to synthetize SMs as donors.[24,25] Alternatively, triple-layer vacuum-processed OSCs based on relatively simple SMs demonstrate outstanding efficiencies of >11%.[26]

The efficiency of OSCs is determined by three parameters:[27] the open-circuit voltage (V_{OC}), the short-circuit current (J_{SC}) and the fill factor (FF), which have to be maximized to achieve the best device performance. Short-circuit current is typically improved by maximizing the amount of collected photons, and maximal FF requires elaborate device engineering to reduce the recombination processes.[28] To maximize the V_{OC}, energy losses have to be minimized by, e.g., matching at best the energy levels of the donor and acceptor materials,[29] lowering the exciton binding energy,[30] increasing state delocalization,[5] reducing energy disorder of the materials,[31] minimizing the recombination via interfacial CT states,[32] etc.[33]

Recently, it was shown that simple SMs with a star-shaped architecture (SSMs) fulfil most requirements for high-efficiency solar cells, with efficiencies >5% demonstrated.[13] The donor core and acceptor end groups ensure broad absorption in the visible region, which results in J_{SC} of >8 mA cm^{-2}, while the star-shaped structure assists column-like self-assembling in the films, thereby enhancing charge transport properties and leading to FF >50%.[1,4,14,34–39] Finally, SSMs-based OSCs demonstrate high V_{OC} of >0.9 V[2,14] in mixture with [70]PCBM, the reason of which is not yet understood. To put it in the perspective, V_{OC} of archetypical P3HT:[70]PCBM OSCs hardly exceeds 0.6 V[40–42] even though the SSMs have similar highest occupied molecular orbital (HOMO) level

O. V. Kozlov, Dr. M. S. Pshenichnikov
Zernike Institute for Advanced Materials
University of Groningen
Nijenborgh 4, 9747 AG Groningen, The Netherlands
E-mail: m.s.pchenitchnikov@rug.nl
Dr. Y. N. Luponosov, A. N. Solodukhin,
Prof. S. A. Ponomarenko
Enikolopov Institute of Synthetic Polymeric Materials
of the Russian Academy of Sciences
Profsoyuznaya st. 70, 117393 Moscow, Russia
B. Flament, Dr. Y. Olivier, Prof. R. Lazzaroni, Prof. J. Cornil
Service de Chimie des Materiaux Nouveaux
Université de Mons
Place du Parc 20, 7000 Mons, Belgium
Prof. S. A. Ponomarenko
Chemistry Department
Lomonosov Moscow State University
Leninskie Gory 1-3, 119991 Moscow, Russia

DOI: 10.1002/adom.201700024

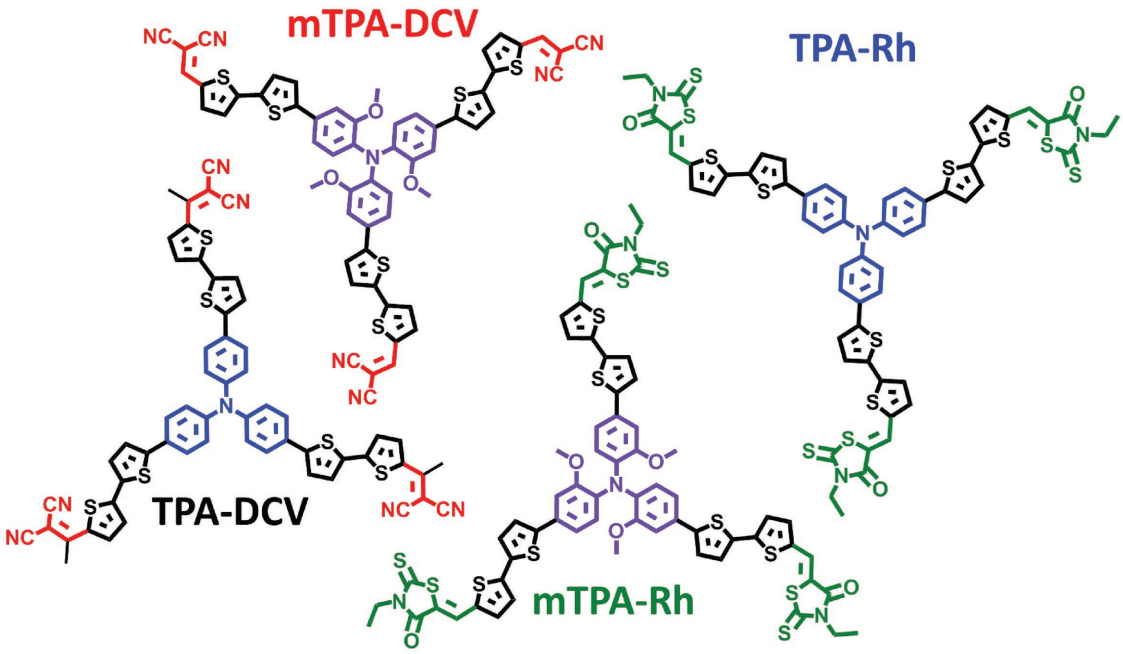

Figure 1. Chemical structures and notations of the SSMs studied.[14] The notations reflect the donor and acceptor units used: triphenylamine (TPA) or *tris*(2-methoxyphenyl)amine (mTPA) as donor core and dicyanovinyl or methyldicyanovinyl (both denoted as DCV) or rhodanine (Rh) as acceptor end groups.

with P3HT (≈5.2–5.3 eV). Therefore, V_{OC} losses (calculated as $(E_{LUMO}^{[70]PCBM} - E_{HOMO}^{Donor})/e\text{-}V_{OC}$, where LUMO stands for lowest unoccupied molecular orbital) amounts to <0.5 V in the OSCs based on the SSMs studied (with the energy level positions taken from Refs. [2,14]), while in P3HT-based OSCs they exceed 0.8 V. Altogether, high J_{SC} and V_{OC} make SSMs perfect benchmark materials for understanding the relations between fundamental photophysics of SM-based OSCs with their performance.

In this work, we used four SSMs[2,14] (**Figure 1**) to understand the early-time photon-to-charge conversion processes in SM-based OCSs. These SSMs comprise different donor (triphenylamine [TPA] or *tris*(2-methoxyphenyl)amine) and acceptor (dicyanovinyl [DCV], methyldicyanovinyl, or rhodanine [Rh]) units (Figure 1) and, therefore, possess different chemical and photophysical properties.[2,14] Despite these major differences in chemical structures, all molecules demonstrate low V_{OC} losses of <0.5 eV and J_{SC} of >8 mA cm^{-2} in bulk heterojunctions (BHJs) with [70]PCBM.[2,14] Using time-resolved photoinduced absorption (PIA) and time-resolved photoluminescence (PL) spectroscopies, we compare the photophysical properties of the molecules diluted in a poly(methyl methacrylate) (PMMA) matrix and strongly interacting molecules in a solid film. We demonstrate that in solid films efficient exciton-to-polaron conversion occurs within the first 100 ps, which leads to the population of the SSM phase with quasi-free charges (polaron pairs). The polaron pairs have lower binding energy compared to excitons and do not fill interfacial charge transfer (CT) states at the donor–acceptor interface, which leads to improved charge collection and lower geminate recombination. Our findings demonstrate that promoting a strong intermolecular coupling between molecules in films is a promising way to increase the OSC efficiency.

2. Experimental Results

2.1. Absorption Spectra

The absorption spectra of the SSMs studied in a PMMA matrix and solid films are shown in **Figure 2**. The low-energy absorption peak is mainly caused by an intramolecular CT[3,43] and its position depends strongly on the particular donor–acceptor combination used. In the PMMA matrices, where the intermolecular interactions are absent, the absorption peak position varies from 499 nm (2.48 eV) for TPA–DCV to 526 nm (2.35 eV) for methoxy-triphenylamine (mTPA)–DCV. The peak for mTPA–Rh molecule lies between the peaks for mTPA–DCV and TPA–Rh. These differences are explained by the fact that the absorption peak reflects the transition energy to an intramolecular CT[3] and therefore depends not on the donor and acceptor units per se but on their combination. The high-energy absorption shoulder has a mixed π–π^* and CT character[3] and also exhibits prominent dependence on the molecular structure. These trends in the absorption spectra are confirmed (even though to a smaller extent than observed experimentally) by the time-dependent (TD)–density functional theory (DFT) calculations (Figure 2, shaded contours).

For all molecules, the absorption spectra in films are red-shifted and broadened compared to the spectra in the matrices. The shift varies from 0.12 eV for TPA–DCV to 0.20 eV for mTPA–DCV. As a result, in the films the absorption spectra for the different molecules peak almost at the same wavelength. The reason is twofold: first, in the solid films, the effect of local dielectric environment[44–47] is more prominent compared to the isolated molecules in PMMA matrix as evidenced from the increased peak widths (≈0.25 eV in PMMA matrix vs ≈0.3 eV in

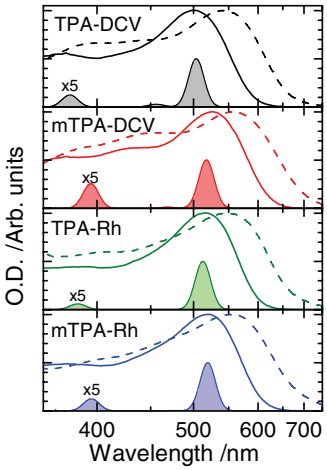

Figure 2. Absorption spectra of the SSMs measured in a PMMA matrix (lines) and in solid films (dashed lines) and calculated (shaded contours) at the TD–DFT level. The calculated spectra are systematically red-shifted by 0.3 eV to account for medium effects and/or the deficiencies of DFT when dealing with charge transfer states. Due to the strong difference in the amplitudes, the calculated intensities of the high-energy peaks were multiplied by 5 for representation purposes.

films). Second, the close packing in the solid allows for intermolecular charge separation which also affects the absorption properties. Overall, the complex behavior of absorption spectra suggests the importance of both the specific molecular structure and intermolecular interactions on the photophysical properties of the materials.

2.2. Photoinduced Absorption Spectra

To examine the early-time photophysics of exciton/charge generation, we performed time-resolved PIA experiments. In these measurements, the samples are excited by an ultrashort visible light and the photoinduced response is probed by the delayed infrared (IR) probe pulse. The absorption of the probe pulse is proportional to the number of photogenerated species and therefore the photoinduced dynamics can be easily tracked with common pump-probe experiment.

It should be noted that the nature of the photoinduced species in the isolated molecules and in the films may be substantially different. For well-separated molecules in a neutral matrix (e.g., PMMA), there are no intermolecular interactions. Therefore, only intramolecular excited states (i.e., excitons and/or intramolecular CT excitons in push–pull molecules as considered herein) are formed upon photon absorption. In the films, the molecules are interacting and, hence, additional pathways for the charge separation become open—e.g., intermolecular formation of polaron pairs.[6,48,49] The optical signatures of intramolecular CT excitons and polarons are typically different and, therefore, the nature of the excited states can be spectrally identified.[6]

Figure 3a shows the PIA spectra of the SSMs in a PMMA matrix upon 510 nm excitation (i.e., near the absorption maximum). Since the molecules are well-separated, the spectra reflect the optical signatures of intramolecular excitations: due to the push–pull nature of the molecules, efficient intramolecular charge separation occurs which causes the electron density to be shifted from the donor core to the acceptor units (see Figures S1–S4 in the Supporting Information).

For all molecules, the PIA spectra in the PMMA matrices consist of an extremely broad background, with a more resolved IR peak (with exception of mTPA–DCV). The broad background is assigned to the excited state absorption as many transitions S_1–S_n are allowed from the first excited state to higher-lying excited states while the peak is likely due to the presence of transition(s) with significantly higher oscillator strength(s) compared to the rest of the manifold.

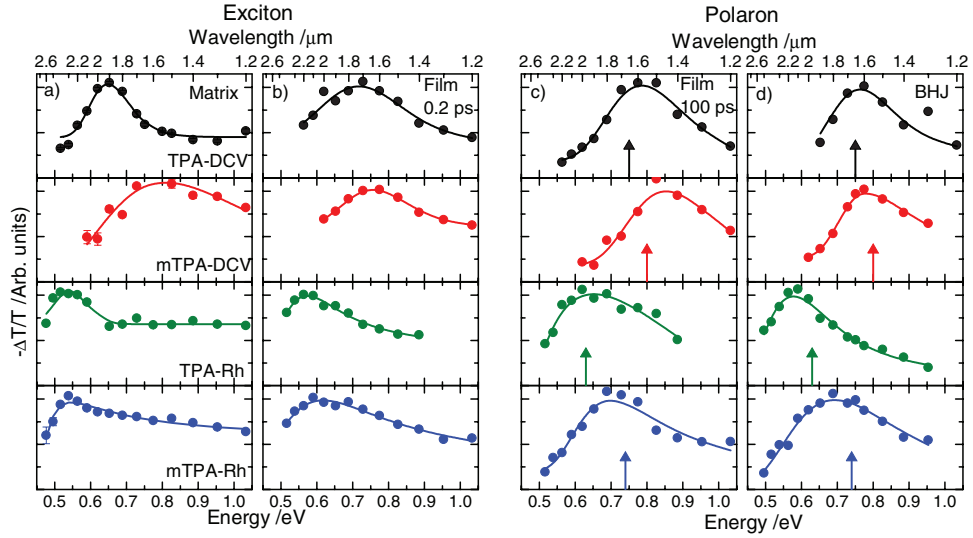

Figure 3. a) PIA spectra of the SSMs studied in a PMMA matrix, b,c) solid films, and d) 1:1 blends with [70]PCBM acceptor upon a) 510 nm or b–d) 550 nm excitation. Symbols represent the experimental data points while solid lines are the best fits with asymmetrical Gaussian functions. The spectra are reconstructed from the PIA transients measured at different wavelengths. The time delays are a) 10 ps, b) 0.2 ps, c,d) 100 ps. Arrows in (c) and (d) show positions of the TD–DFT calculated polaron peaks, systematically red-shifted by 0.2 eV.

Figure 3b,c shows the PIA spectra of the SSMs in solid films at early (0.2 ps) and late (100 ps) delay times. Surprisingly, the spectra are very different at the two delays, indicating a different nature of the photoexcited species. At 0.2 ps delay, the spectra in films resemble those in matrices, indicating photogeneration of intramolecular (CT-)excitons. At 100 ps, the spectra are blue-shifted while the background is significantly reduced in comparison to the 0.2 ps spectra. This is assigned to the formation of the so-called polaron pairs[6,48,49] in the film. The electron and hole of the polaron pair are located on different SSMs (unlike intramolecular CT excitons, where the electron and hole belong to the same molecule), which leads to a reduced Coulomb attraction. On the other hand, the polaron pair is essentially different from the charges located in an interfacial CT state (also called interfacial CT exciton,[50] not to be confused with intramolecular CT excitons), as in the case of the interfacial CT exciton the electron and hole reside on different materials, while the polaron pair is located in the SSM phase. It should be noted that even though no apparent driving force for charge separation is present in the SSM film, the intermolecular charge separation between neighboring SMs is still possible[51,52] because of dense packing. If the donor unit of one molecule is in close proximity to the acceptor unit of the neighboring molecule, intermolecular CT becomes energetically favorable,[3,53] and a polaron pair is formed upon photoexcitation.

Even though the polaron pairs have similar spectroscopic signatures with isolated polarons (charges),[6] they cannot be considered as free charges because (i) the electron and hole still belong to same material and (ii) Coulomb attraction is still significantly higher than kT. Spectroscopically, if the number of intermolecularly separated charges is high, the PIA response should follow the absorption spectra of polarons and not of the intramolecular (CT-)excitons.

To verify this assumption, we measured the PIA response of 1:1 BHJ films of the SSMs with the [70]PCBM electron acceptor, where complete charge separation is known to occur within first 100 ps (Figure 3d) and therefore the PIA response is caused solely by the positive hole polarons (the negative electron polarons on [70]PCBM do not produce a signal in near-IR). As there is a reasonable match between the two sets of spectra, one can conclude that the PIA response of the neat SSM films at long delays is mainly driven by polarons.

The positions of the polaron absorption peaks are different for the different SSMs: the Rh-based molecules exhibit red-shifted absorption compared to the DCV-based SSMs. This can be explained by a longer conjugation length of the Rh-based molecules and, therefore, by a larger delocalization of the charge and a weaker degree of local geometric distortions. In contrast, the methoxy substituents on the mTPA core do not change the conjugation length with respect to TPA; therefore, the polaron peak positions are expected to be similar for the TPA and mTPA-based molecules. This is, however, not the case: the polaron peak positions for the mTPA-based SSMs are in fact blue-shifted compared to the TPA-based molecules. This is attributed to an increased localization of the positive charge around the core in mTPA-based molecules, due to the dominant electron-donating character of the methoxy groups. As a result, the spectrum for the mTPA–Rh molecule is intermediate between the spectra for the TPA–Rh and mTPA–DCV molecules. This counterintuitive behavior is fully captured by the TD–DFT calculations (Figure 3c,d, vertical lines) and highlights the major influence of the particular donor–acceptor combination on the photophysical properties of the material.

2.3. Photoinduced Dynamics

To examine the exciton and polaron dynamics, we studied the time-dependent PIA and PL of SSMs in PMMA matrices and neat films. The PL dynamics of the SSM molecules in PMMA matrices are shown in **Figure 4**a by solid symbols. For all molecules, the PL decays biexponentially: ≈20% of the initial PL decays at hundreds ps timescale, while the rest of PL decays at >2 ns time. The slow decay reflects the radiative lifetime of

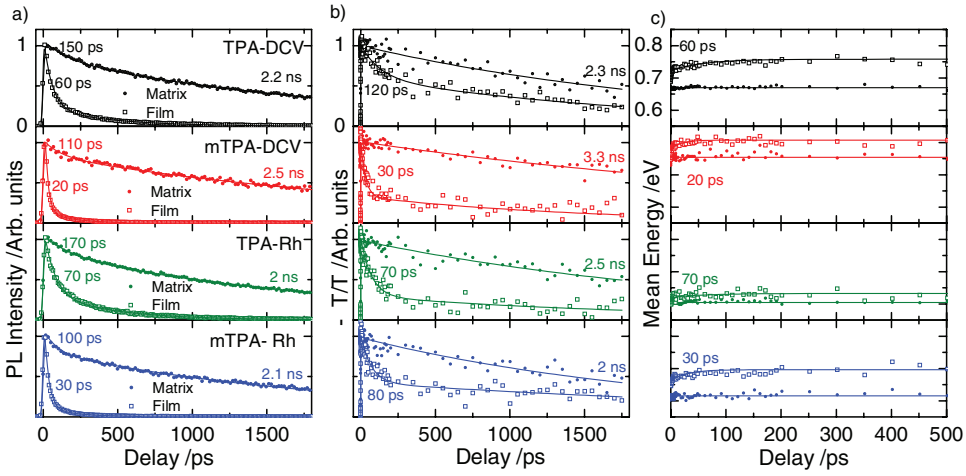

Figure 4. a) PL and b) PIA dynamics and c) shift of the mean energy of the PIA spectra for SSMs in PMMA matrices (solid symbols) and films (open symbols). Experimental points are shown by symbols, solid lines are the best fits with (bi)exponential functions. Excitation wavelengths were 510 nm (matrices) and 550 nm (films), probe wavelengths were set to the maxima of the respective PIA responses (Figure 3a,c). The transients in (a,b) are normalized by their maxima. The numbers show the timescale of the respective processes. PL is integrated in 580–850 nm region (Figure S6, Supporting Information).

the intramolecular (CT-)excitons. The fast decay is ascribed to torsional deformation of the molecules upon photoexcitation.[53] For mTPA-based molecules, the decay is considerably faster compared to the TPA-based derivatives due to the higher floppiness imparted by the methoxy groups: the calculated difference in angle between benzene ring in the donor core and the plane of the molecule in ground and charged state is ≈6° for the mTPA-based molecules and only ≈1° for the TPA-based compounds (Table S1, Supporting Information).

The PIA signals in all SSMs decay with a single exponential time of several nanoseconds: mTPA–DCV SSM produces the longest lifetime of 3.3 ns while the mTPA–Rh exhibits the shortest lifetime of 2 ns. Since the excited state lifetime depends on the transition energy and the transition dipole moment, it is not surprising that the lifetimes are different for different molecules. Note that even though the torsional deformation leads to some PL quenching, the molecule remains in the excited state as no fast decay is observed in PIA measurements (Figure 4b, solid symbols).

In the solid films, both PL and PIA signals decay significantly faster compared to the isolated molecules (Figure 4). 70%–95% of PL decays within first 20–70 ps in the SSM films (Figure 4a, open symbols), indicating fast depletion of the exciton population either via decay to the ground state or dissociation into polarons. In contrast, the PIA signals last much longer and demonstrate biexponential dynamics with the fast part decaying within tens of ps and the slow part decaying on the nanosecond timescale (Figure 4b, open symbols). The fast component of the PIA signal is generally slower as compared to the PL decay time. This indicates interconversion of the initially photogenerated excitons to the polaron pairs, which slows down the decay of the PIA signals probed at the polaron response maxima.

To verify this assumption, we measured the dynamical shift of the PIA spectra (Figure 4c): since the response of intramolecular (CT-)excitons is red-shifted compared to the polaron response, a dynamical blue-shift of the spectrum is expected when the relative share of the polaron pairs increases. This is indeed the case: the PIA spectra gradually shift to higher energies in all studied films, and the shift is more prominent for the molecules where polaron and exciton responses are better separated (e.g., for TPA–DCV and mTPA–Rh). The spectral dynamics at the timescale of tens of ps perfectly match the PL decay times in films, which is in line with the assumption of exciton-to-polaron conversion. Note that the magnitude of spectral diffusion is correlated with the PIA decay times probed at polaron absorption maxima: for the compounds with prominent energy shift (i.e., TPA–DCV and mTPA–Rh) the PIA decay is considerably slower compared to the PL decay (Figure 4). This is due to the interplay between exciton and polaron responses in the PIA signal. As the exciton PIA response is red-shifted compared to the polaron response (Figure 3), at the early timescales the maximum of PIA spectra is blue-shifted relative to the probe wavelength, i.e., the probe wavelength is detuned from the precise resonance. At the later timescales, the exciton response decreases in amplitude, and the polaron response becomes prevailing. The maximum of the PIA spectrum shifts toward the probe wavelength making it on-resonance. Therefore, the decay times of PIA signal probed at the polaron maximum is determined by two factors: (i) depopulation of the excited state (be it polarons or excitons) and (ii) dynamical spectral response due to the exciton-to-polaron conversion.

The exciton-to-polaron conversion is further supported by the fast decay of the photoinduced anisotropy in SSM films (Figure S5, Supporting Information) as the transition dipole moments of the polaron pairs are not necessary correlated with the polarization of the excitation light. Furthermore, in the solid films the excitation migrates within the material, herewith losing the correlation with the polarization of the incident light.

From the PL and PIA measurements, we conclude that after 20–70 ps, the SSM films are populated mainly by polaron pairs and not by excitons. Moreover, high amplitude of fast PL decay and similarity of PIA spectra of neat films and BHJ blends suggest very high (>70%) exciton-to-polaron conversion efficiency. This is beneficial for the OSC operation as the binding energy of intermolecular polaron pairs is lower compared to the exciton binding energy due to the larger separation of the electron and the hole. This echoes the previously proposed scenario that relies on the importance of wavefunction delocalization (to increase the electron–hole separation) for efficient charge separation.[5] We further speculate that the formation of polaron pair instead of excitons likely leads to reduced filling of the interfacial CT states in the BHJs. In the case of an intermolecular polaron pair, the electron and hole belong to different donor molecules in the donor phase and, therefore, after electron transfer to an acceptor (e.g., [70]PCBM) the electron and hole are well-separated spatially. This effectively prevents formation of interfacial CT excitons where electron and hole are located at the adjusting donor and acceptor molecules at the interface. Consequently, the high V_{OC} (>0.5 eV) and J_{SC} (>8 A cm^{-2}) in SSM-based OSCs[14] may be attributed both to the decreased Coulomb attraction between electron and hole (and, therefore, increased charge collection) and reduced CT state recombination.

3. Conclusions

In this work, we studied the early time charge photogeneration in conjugated small molecules. As benchmark systems, four SSMs with two different donor cores: TPA and mTPA, and DCV or methyldicyanovinyl and Rh acceptor groups were selected. To separate the intrinsic properties of the molecules and the collective effects, the photophysical responses of molecules isolated in a PMMA matrix and closely packed in solid films were compared.

The linear absorption of the separated molecules depends on the particular donor–acceptor combination used: the absorption peak position varies from 499 to 526 nm, which is rationalized by the TD–DFT calculations. In the solid films, however, the absorption properties of the different molecules are almost similar and, therefore, are highly determined by collective effects.

For the isolated molecules, the excited state lifetime varies from 2 ns (mTPA–Rh-based molecule) to 3.5 ns (mTPA–DCV-based molecule), which is mainly determined by the radiative lifetime of the excitons. In the films, the radiative lifetime shortens significantly due to dissociation of the excitons into polaron pairs. The formation of polaron pairs is beneficial for

the OSC operation as the Coulomb attraction between intermolecular electron–hole pair is significantly lower compared to the intramolecular exciton. In addition, as the electron and hole in the polaron pair are located at different molecules (although of the same donor phase), a reduced amount of interfacial CT excitons is expected to be formed after electron transfer to the acceptor. These lead to improved charge collection and reduced recombination in SMs-based solar cells. Therefore, enhancing the intermolecular interactions to promote exciton-to-polaron conversion appears to be a promising way towards efficiency optimization.

4. Experimental Section

Sample Preparation: The SSMs were synthesized as described previously in Ref. [2] for TPA–DCV, in Ref. [14] for TPA–Rh and m-TPA–Rh, and in Ref. [54] for m-TPA–DCV. All SSMs were separately dissolved in *ortho*-dichlorobenzene at a concentration of 10 g L^{-1}, PMMA (Sigma-Aldrich, M_w = 120 000 g mol^{-1}) was dissolved in *ortho*-dichlorobenzene at a concentration of 150 g L^{-1}. All solutions were stirred on a magnetic stirrer for at least 12 h at 50 °C. To prepare the separated SSMs in PMMA matrix, PMMA was mixed with the SSMs to achieve 1:50 SSM:PMMA molar ratio (1 SSM per 60 000 PMMA monomer units, ≈20 nm separation between SSMs). Matrix samples and neat films were prepared by drop casting of 150 µL of the solution on microscope cover glass slips. Preparation of the BHJ samples is described elsewhere.[14]

Optical: Absorption spectra were measured with a Lambda-900 spectrometer. The PIA measurements were performed with a setup based on Spectra-Physics Hurricane Ti:Sapphire system and two light Ccnversion TOPAS optical parametric amplifiers, which were used to generate excitation and probe pulses. More detailed description of the PIA setup is given elsewhere.[3]

The isotropic PIA signal and photoinduced anisotropy were recalculated from parallel and perpendicular to the polarization of the excitation pulse PIA components as[55]

$$\Delta T_{iso}(t) = \frac{\Delta T_{||}(t) + 2\times\Delta T_{\perp}(t)}{3} \quad (1)$$

$$r(t) = \frac{\Delta T_{||}(t) - \Delta T_{\perp}(t)}{3\times\Delta T_{iso}} \quad (2)$$

The angle α between polarization of excitation pulse and photoinduced dipole moment was calculated from the anisotropy value r[55]

$$r = r_0\left(1 - \frac{3}{2}\sin^2(\alpha)\right) \quad (3)$$

Time-resolved PL was measured at a Hamamatsu C5680 streak-camera. The excitation wavelengths of 510 and 550 nm were selected from the white light supercontinuum generated from a Mira Ti:sapphire laser output in a Newport SCG-800 hollow fiber.

Computational: The geometry of the neutral and singly positively charged molecules have been fully optimized at the DFT level using the B3LYP functional and a 6-31G** basis set. The optical transition energies have been computed at the TD–DFT level using the same basis set and the BHHLYP functional, which better accounts for charge-transfer properties; the optical spectra have been simulated using a Gaussian broadening of the transition energies, with a full width at half maximum set at 0.2 eV.

Supporting Information

Supporting Information is available from the Wiley Online Library or from the author.

Acknowledgements

O.V.K. acknowledges Aurora—Toward Modern and Innovative Higher Education program for financial support. Studies on conjugated materials in Mons are supported by the Science Policy Office of the Belgian Government (BELSPO; PAI 7/5) and FNRS-FRFC. J.C. is FNRS research director. Y.N.L., A.N.S., and S.A.P. thank Russian Science Foundation (Grant No. 14-13-01380) for financial support of the synthesis of the star-shaped molecules.

Received: January 10, 2017
Revised: January 24, 2017
Published online: March 7, 2017

[1] S. Ponomarenko, Y. Luponosov, J. Min, A. N. Solodukhin, N. Surin, M. Shcherbina, S. N. Chvalun, T. Ameri, C. J. Brabec, *Faraday Discuss.* **2014**, *174*, 313.
[2] J. Min, Y. N. Luponosov, A. Gerl, M. S. Polinskaya, S. M. Peregudova, P. V. Dmitryakov, A. V. Bakirov, M. A. Shcherbina, S. N. Chvalun, S. Grigorian, N. Kaush-Busies, S. A. Ponomarenko, T. Ameri, C. J. Brabec, *Adv. Energy Mater.* **2014**, *4*, 1301234.
[3] O. V. Kozlov, Y. N. Luponosov, S. A. Ponomarenko, N. Kausch-Busies, D. Y. Paraschuk, Y. Olivier, D. Beljonne, J. Cornil, M. S. Pshenichnikov, *Adv. Energy Mater.* **2015**, *5*, 1401657.
[4] Z. M. Tang, T. Lei, J. L. Wang, Y. G. Ma, J. Pei, *J. Org. Chem.* **2010**, *75*, 3644.
[5] A. A. Bakulin, A. Rao, V. G. Pavelyev, P. H. M. van Loosdrecht, M. S. Pshenichnikov, D. Niedzialek, J. Cornil, D. Beljonne, R. H. Friend, *Science* **2012**, *335*, 1340.
[6] R. Tautz, E. Da Como, T. Limmer, J. Feldmann, H.-J. Egelhaaf, E. von Hauff, V. Lemaur, D. Beljonne, S. Yilmaz, I. Dumsch, S. Allard, U. Scherf, *Nat. Commun.* **2012**, *3*, 970.
[7] Q. Zhang, B. Kan, F. Liu, G. Long, X. Wan, X. Chen, Y. Zuo, W. Ni, H. Zhang, M. Li, Z. Hu, F. Huang, Y. Cao, Z. Liang, M. Zhang, T. P. Russell, Y. Chen, *Nat. Photonics* **2015**, *9*, 35.
[8] W. Ni, M. Li, F. Liu, X. Wan, H. Feng, B. Kan, Q. Zhang, H. Zhang, Y. Chen, *Chem. Mater.* **2015**, *27*, 6077.
[9] K. Kawashima, Y. Tamai, H. Ohkita, I. Osaka, K. Takimiya, *Nat. Commun.* **2015**, *6*, 10085.
[10] Q. An, F. Zhang, Q. Sun, J. Wang, L. Li, J. Zhang, W. Tang, Z. Deng, *J. Mater. Chem. A* **2015**, *3*, 16653.
[11] G. J. Hedley, A. J. Ward, A. Alekseev, C. T. Howells, E. R. Martins, L. A. Serrano, G. Cooke, A. Ruseckas, I. D. W. Samuel, *Nat. Commun.* **2013**, *4*, 2867.
[12] M. S. Siraj, *Synth. Commun.* **2012**, *42*, 1922.
[13] J. Min, Y. N. Luponosov, Z.-G. Zhang, S. A. Ponomarenko, T. Ameri, Y. Li, C. J. Brabec, *Adv. Energy Mater.* **2014**, *4*, 1400816.
[14] Y. N. Luponosov, J. Min, A. N. Solodukhin, O. V. Kozlov, M. A. Obrezkova, S. M. Peregudova, T. Ameri, S. N. Chvalun, M. S. Pshenichnikov, C. J. Brabec, S. A. Ponomarenko, *Org. Electron.* **2016**, *32*, 157.
[15] M. Schwarze, W. Tress, B. Beyer, F. Gao, R. Scholz, C. Poelking, K. Ortstein, A. A. Günther, D. Kasemann, D. Andrienko, K. Leo, *Science* **2016**, *352*, 1446.
[16] S. Torabi, F. Jahani, I. Van Severen, C. Kanimozhi, S. Patil, R. W. A. Havenith, R. C. Chiechi, L. Lutsen, D. J. M. Vanderzande, T. J. Cleij, J. C. Hummelen, L. J. A. Koster, *Adv. Funct. Mater.* **2015**, *25*, 150.

[17] J. Roncali, P. Leriche, P. Blanchard, *Adv. Mater.* **2014**, *26*, 3821.
[18] Y. Liu, Y. M. Yang, C. C. Chen, Q. Chen, L. Dou, Z. Hong, G. Li, Y. Yang, *Adv. Mater.* **2013**, *25*, 4657.
[19] L. Li, L. Xiao, H. Qin, K. Gao, J. Peng, Y. Cao, F. Liu, T. P. Russell, X. Peng, *ACS Appl. Mater. Interfaces* **2015**, *7*, 21495.
[20] B. Walker, C. Kim, T. Q. Nguyen, *Chem. Mater.* **2011**, *23*, 470.
[21] Y. Lin, Y. Li, X. Zhan, *Chem. Soc. Rev.* **2012**, *41*, 4245.
[22] K. Do, C. Kim, K. Song, S. J. Yun, J. K. Lee, J. Ko, *Sol. Energy Mater. Sol. Cells* **2013**, *115*, 52.
[23] J. W. Choi, C.-H. Kim, J. Pison, A. Oyedele, D. Tondelier, A. Leliege, E. Kirchner, P. Blanchard, J. Roncali, B. Geffroy, *RSC Adv.* **2014**, *4*, 5236.
[24] B. Kan, M. Li, Q. Zhang, F. Liu, X. Wan, Y. Wang, W. Ni, G. Long, X. Yang, H. Feng, Y. Zuo, M. Zhang, F. Huang, Y. Cao, T. P. Russell, Y. Chen, *J. Am. Chem. Soc.* **2015**, *137*, 3886.
[25] Y. Liu, C.-C. Chen, Z. Hong, J. Gao, Y. Yang, H. Zhou, L. Dou, G. Li, Y. Yang, *Sci. Rep.* **2013**, *3*, 3356.
[26] X. Che, X. Xiao, J. D. Zimmerman, D. Fan, S. R. Forrest, *Adv. Energy Mater.* **2014**, *4*, 1400568.
[27] Y.-W. Su, S.-C. Lan, K.-H. Wei, *Mater. Today* **2012**, *15*, 554.
[28] M.-H. Jao, H.-C. Liao, W.-F. Su, *J. Mater. Chem. A* **2016**, *4*, 5784.
[29] I. Lange, J. Kniepert, P. Pingel, I. Dumsch, S. Allard, S. Janietz, U. Scherf, D. Neher, *J. Phys. Chem. Lett.* **2013**, *4*, 3865.
[30] S. Y. Leblebici, T. L. Chen, P. Olalde-Velasco, W. Yang, B. Ma, *ACS Appl. Mater. Interfaces* **2013**, *5*, 10105.
[31] J. C. Blakesley, D. Neher, *Phys. Rev. B* **2011**, *84*, 075210.
[32] K. Vandewal, K. Tvingstedt, A. Gadisa, O. Inganas, J. V. Manca, *Nat. Mater.* **2009**, *8*, 904.
[33] N. K. Elumalai, A. Uddin, *Energy Environ. Sci.* **2016**, *9*, 391.
[34] D. Dan, S. Suling, Z. Jing, H. Chang, Z. Zhanjun, L. Yongfang, *Org. Electron.* **2012**, *13*, 2546.
[35] J. Zhang, D. Deng, C. He, Y. He, M. Zhang, Z.-G. Zhang, Z. Zhang, Y. Li, *Chem. Mater.* **2011**, *23*, 817.
[36] H. X. Shang, H. J. Fan, Y. Liu, W. P. Hu, Y. F. Li, X. W. Zhan, *Adv. Mater.* **2011**, *23*, 1554.
[37] Z. H. Lin, J. Bjorgaard, A. G. Yavuz, M. E. Kose, *J. Phys. Chem. C* **2011**, *115*, 15097.
[38] J. Zhang, D. Deng, C. He, Y. He, M. Zhang, Z.-G. Zhang, Z. Zhang, Y. Li, *Chem. Mater.* **2010**, *23*, 817.
[39] N. Metri, X. Sallenave, L. Beouch, C. Plesse, F. Goubard, C. Chevrot, *Tetrahedron Lett.* **2010**, *51*, 6673.
[40] F. Zhang, Z. Zhuo, J. Zhang, X. Wang, X. Xu, Z. Wang, Y. Xin, J. Wang, J. Wang, W. Tang, Z. Xu, Y. Wang, *Sol. Energy Mater. Sol. Cells* **2012**, *97*, 71.
[41] C.-W. Chu, H. Yang, W.-J. Hou, J. Huang, G. Li, Y. Yang, *Appl. Phys. Lett.* **2008**, *92*, 103306.
[42] Y. Toshihiro, T. Tetsuya, S. Jun, S. Kazuhiro, *Jpn. J. Appl. Phys.* **2008**, *47*, 1230.
[43] E. Ripaud, Y. Olivier, P. Leriche, J. Cornil, J. Roncali, *J. Phys. Chem. B* **2011**, *115*, 9379.
[44] H. van Eersel, R. A. J. Janssen, M. Kemerink, *Adv. Funct. Mater.* **2012**, *22*, 2700.
[45] L. Goris, A. Poruba, L. Hod'akova, M. Vanecek, K. Haenen, M. Nesladek, P. Wagner, D. Vanderzande, L. De Schepper, J. V. Manca, *Appl. Phys. Lett.* **2006**, *88*, 052113.
[46] R. Coehoorn, W. F. Pasveer, P. A. Bobbert, M. A. J. Michels, *Phys. Rev. B* **2005**, *72*, 155206.
[47] G. M. Akselrod, F. Prins, L. V. Poulikakos, E. M. Y. Lee, M. C. Weidman, A. J. Mork, A. P. Willard, V. Bulović, W. A. Tisdale, *Nano Lett.* **2014**, *14*, 3556.
[48] J. G. Muller, J. M. Lupton, J. Feldmann, U. Lemmer, M. C. Scharber, N. S. Sariciftci, C. J. Brabec, U. Scherf, *Phys. Rev. B* **2005**, *72*, 195208.
[49] Z. Xu, B. Hu, *Adv. Funct. Mater.* **2008**, *18*, 2611.
[50] A. E. Jailaubekov, A. P. Willard, J. R. Tritsch, W.-L. Chan, N. Sai, R. Gearba, L. G. Kaake, K. J. Williams, K. Leung, P. J. Rossky, X. Y. Zhu, *Nat. Mater.* **2013**, *12*, 66.
[51] U. B. Cappel, D. Moia, A. Bruno, V. Vaissier, S. A. Haque, P. R. F. Barnes, *Sci. Rep.* **2016**, *6*, 21276.
[52] X. He, G. Zhu, J. Yang, H. Chang, Q. Meng, H. Zhao, X. Zhou, S. Yue, Z. Wang, J. Shi, L. Gu, D. Yan, Y. Weng, *Sci. Rep.* **2015**, *5*, 17076.
[53] E. Salamatova, O. V. Kozlov, Y. N. Luponosov, A. N. Solodukhin, V. Y. Toropynina, S. A. Ponomarenko, M. S. Pshenichnikov, *Proc. SPIE* **2016**, *9923*, 99230K.
[54] Y. N. Luponosov, J. Min, A. N. Solodukhin, A. V. Bakirov, P. V. Dmitryakov, M. A. Shcherbina, S. M. Peregudova, G. V. Cherkaev, S. N. Chvalun, C. J. Brabec, S. A. Ponomarenko, *J. Mater. Chem. C* **2016**, *4*, 7061.
[55] R. G. Gordon, *J. Chem. Phys.* **1966**, *45*, 1643.